MATERIALS CHEMISTRY FRONTIERS

RESEARCH ARTICLE

View Article Online
View Journal | View Issue

Cite this: *Mater. Chem. Front.*, 2023, **7**, 1385

Nano-polyaniline enables highly efficient electrocatalytic reduction of CO_2 to methanol in supporting electrolyte-free media and the detection of free-radical signals

Shaolin Mu, *[a] Qiaofang Shi,[a] Chong Chen,[b] Xiangxiang Gong[b] and Huaiguo Xue[a]

Received 31st October 2022,
Accepted 9th February 2023

DOI: 10.1039/d2qm01119k

rsc.li/frontiers-materials

Metals and metal oxides are widely used as catalysts for the electrochemical reduction of CO_2. Here, we report a low-cost catalyst based on nano-polyaniline polymerized on graphite for the electrochemical reduction of CO_2 in CO_2-saturated water free of supporting electrolytes. The nano-polyaniline electrode in this solution shows low resistance and low charge-transfer impedance (R_{ct}), which leads to a rather high reduction current density (−16.8 mA cm^{-2}) and low overpotential (−0.44 V *vs.* Ag/AgCl). This solution is environment-friendly and mimics that in photosynthesis. The free radical signal of CO_2 was successfully detected during the reduction process. The ^1H NMR result demonstrates that the only product formed was methanol.

Introduction

The continuous rise in CO_2 levels in the atmosphere has led to global warming and environmental contamination. The electrochemical reduction of carbon dioxide ($ERCO_2$) can possibly reduce greenhouse gas emissions and also produce value-added chemicals, such as CH_3OH,[1–5] formate,[6–8] HCOOH,[9–12] C_2H_5OH,[13,14] CH_3COOH,[15] and CO.[16] In addition, the $ERCO_2$ can be easily controlled by modulating the applied potential, and the reaction is carried out under mild conditions. However, CO_2 is a very stable molecule because of the high energy of the C═O bond. This means that the $ERCO_2$ needs the presence of catalysts to decrease the reaction energy barrier. On the basis of previous reports,[17,18] various catalysts, such as metals,[19–23] metal complexes,[24] metal oxides,[25–28] and semiconductors,[29] have been used for the $ERCO_2$. Conducting polymers are also promising candidates due to their good redox properties, low cost and facile processing. However, the use of conducting polymers as catalysts for efficient $ERCO_2$ has rarely been reported, whereas conducting polymers have only been used as carriers of the catalysts.[15,30] Among these, Cu-based catalysts and ultrathin metal catalysts have aroused considerable interest due to the fact that Cu-based catalysts exhibit good selectivity (80%)[31] and high faradaic efficiency from 43% to 62%,[3,25,31] and ultrathin metal catalysts exhibit high catalytic activity (−13 mA cm^{-2} to −21.2 mA cm^{-2}) and lower overpotentials (−0.24 V *vs.* SCE).[32–34]

In addition, transition-metal-based nanomaterials have also been used for the electrochemical reduction of CO_2.[35] For instance, ionomers, MXenes, conducting polymers and their graphene composites have shown excellent electrochemical properties.[36–38]

Suitable catalysts for the $ERCO_2$ must be environment-friendly and exhibit high electrocatalytic activity, selectivity, stability and a low overpotential. Therefore, scientists are facing tough challenges and still have a long way to go toward developing ideal catalysts for $ERCO_2$, even in terms of electrocatalytic activity and product selectivity.

$NaHCO_3$[19,20] and $KHCO_3$,[4,8,34] which play an important role in enhancing the solution conductivity, are usually used as supporting electrolytes in CO_2 electroreduction. However, the presence of the supporting electrolytes is unfavorable for the analysis and direct application of the product solution; moreover, Na^+ or K^+ in the double layer affect the migration of H^+ in the solution.[39]

The aniline copolymer deposited on fluorine-doped tin oxide (FTO) glass could catalyze the $ERCO_2$ in water free of supporting electrolytes,[40] but its catalytic activity was lower than those of Cu-based catalysts and ultrathin metal catalysts used in solutions containing supporting electrolytes; the low conductivity of FTO and water led to very low current density during CO_2 reduction despite good pH dependence. Here, we report polyaniline (PAn) as a catalyst for the $ERCO_2$, along with graphite sheet as the polyaniline carrier to form the PAn/graphite electrode.

[a] *School of Chemistry and Chemical Engineering, Yangzhou University, Yangzhou 225002, Jiangsu Province, P. R. China. E-mail: slmu@yzu.edu.cn*
[b] *Testing Center of Yangzhou University, Yangzhou, 225002, Jiangsu Province, P. R. China*

The $ERCO_2$ occurs at the gas–liquid–solid interfaces of the electrode, so the electrode wettability plays a pivotal role in the $ERCO_2$ efficiency[41] because the affinity of the electrode surface for aqueous solutions strongly affects the solid–liquid contact angle and thereby impacts electrode activity toward the $ERCO_2$. Herein, we found that the PAn/graphite electrode possesses extremely good wettability.

The nano-PAn/graphite electrode exhibited high selectivity, electrocatalytic activity and low overpotential toward the $ERCO_2$ compared with the aniline copolymer/FTO electrode in water free of supporting electrolytes, which is attributed to the high conductivity of graphite and polyaniline, as well as the surface roughness, large specific surface area and extremely high wettability of polyaniline. An aniline copolymer electrode was prepared by the electrochemical copolymerization of aniline and 2-amino-4-hydroxybenzenesulfonic acid on a fluorine-doped tin oxide (FTO) glass. This copolymer shows good pH-dependence, but its electric conductivity is lower than that of polyaniline.[40]

Experimental section

Chemicals and materials

High-purity carbon dioxide gas (>99.999%) and double-distilled water were used for the $ERCO_2$. Aniline was distilled under reduced pressure before use. Graphite sheets were purchased from Foshan Yinyihui Mould Co., Ltd and are denoted as N-graphite sheets. The N-graphite sheet was treated with a solution consisting of 8.1 M H_2SO_4 and 0.085 M $K_2Cr_2O_7$ for a few minutes, depending on the graphite nature. The treated N-graphite sheet loses its hydrophobic character and is called the T-graphite sheet in this work.

Synthesis of polyaniline and the electrochemical reduction of carbon dioxide

A traditional three-electrode cell consisting of a graphite sheet working electrode, a Pt foil counter electrode and a saturated calomel electrode (SCE) was used for the electrochemical synthesis of polyaniline. The aniline solution consisted of 0.2 M aniline and 0.6 M H_2SO_4; the polyaniline film was deposited on a graphite sheet (1 cm^2) to form the PAn/graphite electrode unless the area of the graphite sheet is mentioned otherwise. The $ERCO_2$ was carried out on a three-electrode system consisting of a PAn/graphite working electrode, a Pt foil counter electrode and Ag/AgCl (with saturated KCl solution) as the reference electrode. For the $ERCO_2$, double-distilled water was saturated by bubbling CO_2 for 20 min prior to measurement, and then, a continuous flow of CO_2 was maintained over the solution during electroreduction. The carbon dioxide molecules in water dissociated into H^+ and HCO_3^- ions to form a weak electrolyte solution.

$$CO_2 + H_2O \rightleftharpoons H^+ + HCO_3^-$$

The conductivity of the CO_2-saturated water was $\sim$20 μS cm^{-1} (pH 3.8).

All the electrochemical measurements were performed on a CHI 611C workstation. The impedance of the PAn/graphite electrode was determined under the given potential in the CO_2-saturated water solution free of supporting electrolytes in the frequency range of 10^5–0.01 Hz.

Physical characterization of the polyaniline catalyst

The N-graphite sheet and the polyaniline/N-graphite sheet were observed using a scanning electron microscope (Gemini SEM 300 instrument). An HT 7800 model transmission electron microscope was used to obtain the TEM images of the polyaniline catalyst. The roughness of the electrode surface was investigated using the Bruker Multimode 8 Atomic Force Microscope (AFM. German). The specific surface area of the graphite samples was measured on a specific surface and pore size analysis instrument (BeiShiDe). The measurement of contact angles was carried out on the contact angle instrument JC20003D3. The measurement of electron spin resonance (ESR) was carried out on a Bruker A300 spectrometer operating in X-band (9.862 GHz) at 25 °C. The Bruker Company provided a *g*-factor marker with $S^{3/2}$. A home-made electrochemical ESR cell was used for the *in situ* electrochemical-ESR studies similar to a previous study,[42] but both working and counter electrodes were inserted into the very thin glass capillary of the ESR cell for studying the $ERCO_2$ in this work. The ^1H NMR spectrum of the product solution with D_2O was recorded on a 600 MHz Bruker spectrometer at 303.1 K.

Results and discussion

Synthesis of polyaniline and its electrochemical properties

The cyclic voltammetry method was used for the electrochemical polymerization of aniline. Aniline was polymerized on a porous T-graphite sheet. Fig. 1(a) shows the cyclic voltammogram (CV) of the electrochemical oxidative polymerization of aniline in a 0.6 M H_2SO_4 solution in the potential range of −0.2 V to 1.0 V (SCE). Fig. 1(a) indicates that the redox currents increased very rapidly with the increasing number of cycles. The current density was very large; this is attributed to the high roughness and the large specific surface area of the T-graphite electrode. In this case, only three cycles were enough to prepare the PAn/T-graphite electrode for the study of $ERCO_2$. This electrode was characterized in a 0.2 M H_2SO_4 solution (Fig. 1(b)). There were three pairs of redox peaks with high redox peak currents. The first pair of redox peaks in the 0.0 to 0.25 V range is caused by the doping and de-doping of anions, the third pair of redox peaks between 0.6 and 0.9 V is related to the pH value of the solution, and the middle redox peaks are attributed to the intermediates (oligomer of phenazine). Therefore, the CV in Fig. 1(b) is very similar in shape to that of polyaniline polymerized on a Pt foil in the same solution, which means that the PAn/T-graphite electrode exhibits good redox activity similar to PAn/Pt.[43]

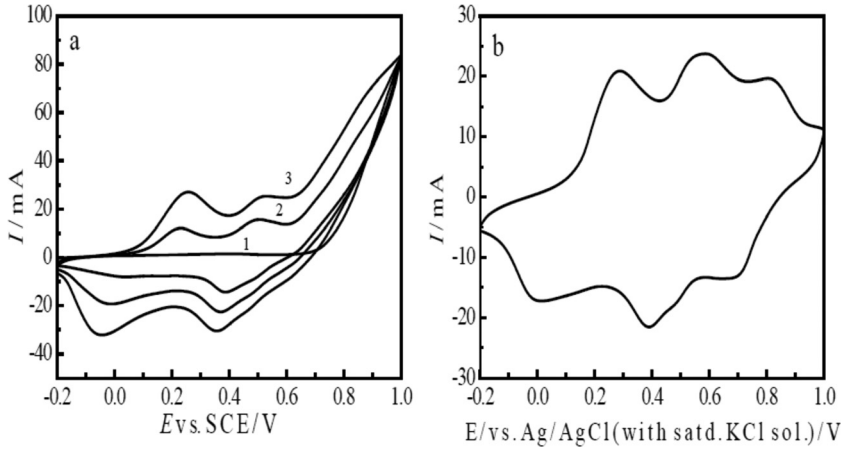

Fig. 1 (a) CVs of the electrochemical synthesis of the polyaniline film on graphite obtained in a solution containing 0.2 M aniline and 0.6 M H_2SO_4; (b) the CV of the polyaniline film in a 0.2 M H_2SO_4 solution at a scan rate of 60 mV s^{-1}.

The redox form of polyaniline synthesized in an HCl solution, as presented by MacDiarmid *et al.*, is as follows:[43]

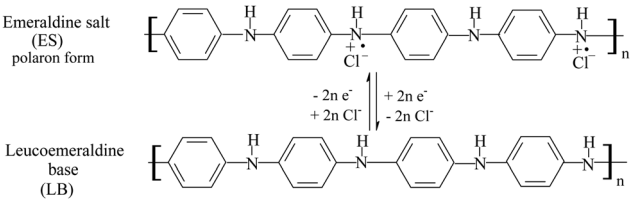

The stable polyaniline radicals can be regarded as the mediators of $ERCO_2$.

Images and specific surface area

The images of the N-graphite sheet, polyaniline deposited on an N-graphite sheet, T-graphite sheet, and polyaniline deposited on a T-graphite sheet are shown in Fig. 2(a-1), (b-1), (a-2) and (b-2), respectively. The image of the N-graphite sheet presented a block-like structure, and the polyaniline film on the N-graphite sheet consisted of fibrils with a length of 250–1000 nm and a diameter of 200 nm. The T-graphite sheet was composed of blocks and fibrils, and the polyaniline film on the T-graphite sheet was made of fibrils with a length of 300–1100 nm and a diameter of 60–120 nm. These results indicate that the polyaniline films consisted of nanofibrils, and the fibril diameter in the polyaniline film on the T-graphite sheet was less than that in the polyaniline film on the N-graphite sheet.

Fig. 2(b) displays the TEM images of T-graphite (Fig. 2(b-1)) and the polyaniline/T-graphite catalyst (Fig. 2(b-2)). The size of T-graphite was about 240 nm × 340 nm, and the size of the polyaniline/T-graphite catalyst was about 111 nm × 330 nm. A comparison of two plots in Fig. 2(b) shows that polyaniline was coated on the surface of the T-graphite grains.

The specific surface areas of the N-graphite sheet and the T-graphite sheet were 0.0134 m^2 g^{-1} and 6.75 m^2 g^{-1}, respectively, that is, the specific surface of the T-graphite sheet was 504 times that of the N-graphite sheet. This demonstrates that after the N-graphite sheet was treated with the concentrated acid and $K_2Cr_2O_7$, its specific surface area dramatically increased.

The relationship between surface roughness and wettability

The roughness of the N-graphite sheet is shown in Fig. 3(a). Its surface roughness (R_g) was 124 nm; however, the roughness of the T-graphite sheet was over 5 μm, which is beyond the measurement limit of the instrument. These results demonstrate that the surface roughness of the T-graphite sheet was much higher than that of the N-graphite sheet.

The change in the contact angle with time was monitored for water on the three different electrode surfaces; the results are shown in Fig. 3(b1)–(b3), respectively. Fig. 3(b1) indicates that the contact angle between water and the N-graphite sheet changed from 134.24° at t = 0 to 79.85° at t = 30 min; Fig. 3(b2) shows that the contact angle between water and the T-graphite sheet changed from 116.88° at t = 0 to 13.88° at t = 13 min. This result indicates that the T-graphite sheet was almost completely wetted in the measuring period of 13 min, which is much faster than the case of the N-graphite sheet. The above results demonstrate that the rough surface is associated with smaller contact angles, which is in good agreement with the relationship between wettability and surface roughness in porous media determined using the X-ray tomography technique.[44] High wettability increases the geometric surface area of the graphite sheet, which is favorable to the electrochemical polymerization of aniline, enhances the surface area of the polyaniline film and the electrocatalytic ability of polyaniline toward the $ERCO_2$, and increases the reduction current density of $ERCO_2$.

Fig. 3(b3) shows the change in contact angle with time for water on the polyaniline film deposited electrochemically on the T-graphite sheet. The results show that polyaniline was almost completely wetted at t = 1 s. This result demonstrates that polyaniline on the T-graphite sheet has very high wettability in water, which increases the surface area of this polyaniline electrode in contact with the solution and shortens the response time of the electrode.

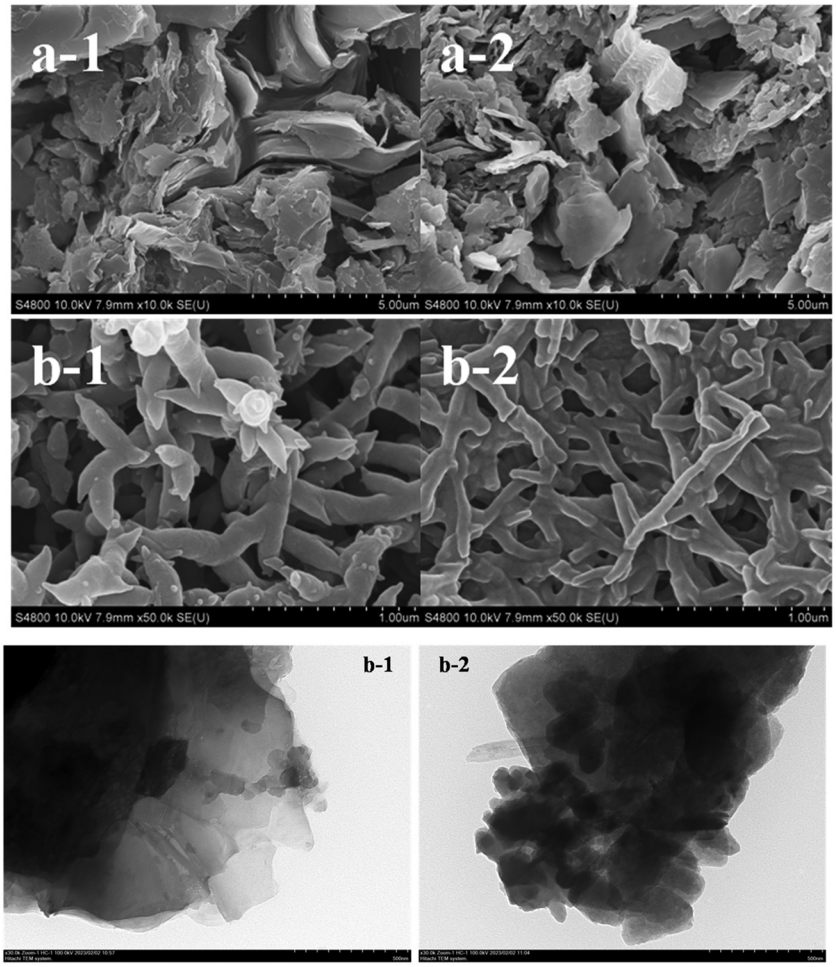

Fig. 2 (a) SEM images: (a-1) N-graphite sheet, (a-2) T-graphite sheet, (b-1) polyaniline film deposited on a N-graphite sheet, (b-2) polyaniline film deposited on a T-graphite sheet. (b) TEM Images: (b-1) T-graphite and (b-2) the polyaniline/T-graphite catalyst.

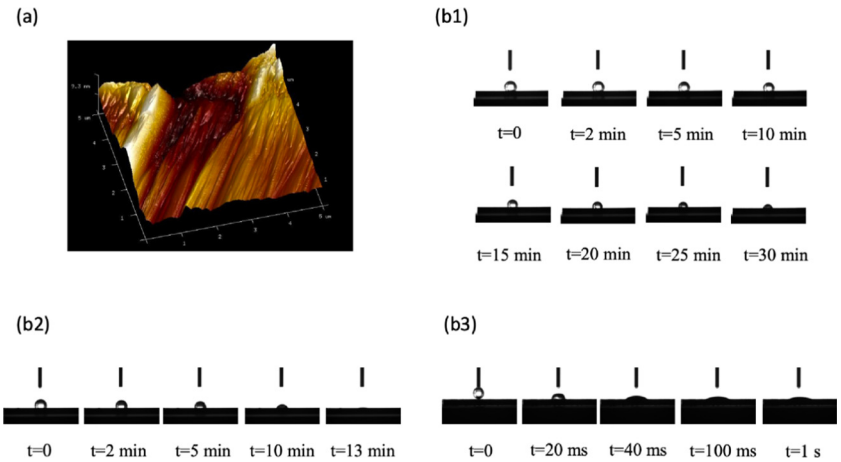

Fig. 3 (a) The surface roughness of the N-graphite sheet. (b) The contact angles as a function of time: (b1) N-graphite sheet, (b2) T-graphite sheet, and (b3) polyaniline film deposited electrochemically on a T-graphite sheet.

The electrochemical reduction of CO_2 in water free of supporting electrolytes

The $ERCO_2$ was first studied using the cyclic voltammetry method, which can provide rapidly a wealth of information, such as the catalyst activity, reduction potentials of CO_2 and charge transfer rate of the electrochemical reduction. Curve 1 in Fig. 4(a) is the CV of the nano-PAn/N-graphite electrode in CO_2-saturated water, showing a CO_2 reduction peak at −0.30 V with a reduction peak current of −3.0 mA (1 cm^2 surface area). Curve 2 in Fig. 4(a) is the CV of the nano-PAn/T-graphite electrode, revealing a reduction peak at −0.25 V and a reduction peak current of −16.42 mA; its electrode surface area is 1.25 cm^2, so the current density is −13.14 mA cm^{-2} at the scan rate of 60 mV s^{-1}. The reduction peak potentials on curve 1 and curve 2 suggest the intrinsic quality of a catalyst. The aniline copolymer/FTO electrode in CO_2-saturated water free of supporting electrolytes showed that the reduction peak current density at the same scan rate was −0.2304 mA cm^{-2}; therefore, the current density of the nano-PAn/T-graphite electrode is 57 times that of the aniline copolymer/FTO electrode.[40]

In addition, the above results indicate that the reduction peak potential of the nano-PAn/T-graphite electrode was lower than that of the nano-PAn/N-graphite electrode, and the reduction peak current density of the nano-PAn/T-graphite electrode was higher than that of the nano-PAn/N-graphite electrode, indicating that the electrocatalytic activity of the nano-PAn/T-graphite electrode was higher than that of the nano-PAn/N-graphite electrode. The reason is that the roughness and specific surface area of the T-graphite sheet are much higher than those of the N-graphite sheet, which leads to a greater contact surface area between aniline and the T-graphite electrode than that between aniline and the N-graphite electrode during the electrochemical polymerization of aniline; furthermore, the polyaniline fibril diameter on the T-graphite surface is less than that on N-graphite surface. As a result, the apparent surface area of polyaniline on the T-graphite sheet electrode is much higher than that on the N-graphite sheet electrode.

To prove that the reduction peaks in curves 1 and 2 of Fig. 4(a) are caused by CO_2 and not polyaniline, the following CV experiments were done. Curve 1 in Fig. 4(b) is the CV of the nano-PAn/T-graphite electrode in a diluted H_2SO_4 solution of pH 3.8, which is equal to that of the CO_2-saturated water solution. The reduction peak was seen at 0.40 V (curve 1 of Fig. 4(b)), which is a much higher potential than that of the peak in curve 1 of Fig. 4(a). This reduction peak is caused by the reduction of polyaniline itself. Curve 2 in Fig. 4(b) is the CV of the bare T-graphite electrode in the CO_2-saturated water solution, with no reduction peak. Clearly, the reduction peaks on curves 1 and 2 in Fig. 4(a) are only caused by the electrochemical reduction of CO_2 on polyaniline, *i.e.*, polyaniline exhibits great catalytic activity in the $ERCO_2$. However, graphite itself did not show any catalytic activity in CO_2 reduction because the $ERCO_2$ is carried out at less negative potentials in our experimental conditions compared to other electrode materials.

Fig. 5(a) shows the CVs of the $ERCO_2$ on the nano-PAn/T-graphite electrode (s = 1.25 cm^2) in CO_2-saturated water free of supporting electrolytes, displaying the reduction peak current and peak potential as functions of the scan rate. The peak current increased from −5.774 mA (its current density was −4.595 mA cm^{-2}) to −21.00 mA (the current density was 16.8 mA cm^{-2}), accompanied by a peak potential shift from 0.086 to −0.44 V when the potential scan rate was increased from 10–400 mV s^{-1}. At the highest scan rate (400 mV s^{-1}), a reduction peak was still observed on the *I–E* curve, indicating the fast charge transfer rate of the electrode reaction and that polyaniline has rather high catalytic activity. The low overpotential effectively inhibits the formation of hydrogen during the reduction process of CO_2. The curves in Fig. 4(a) and 5(a) are very smooth, meaning no observable gas formation at the electrode surface in this potential region.

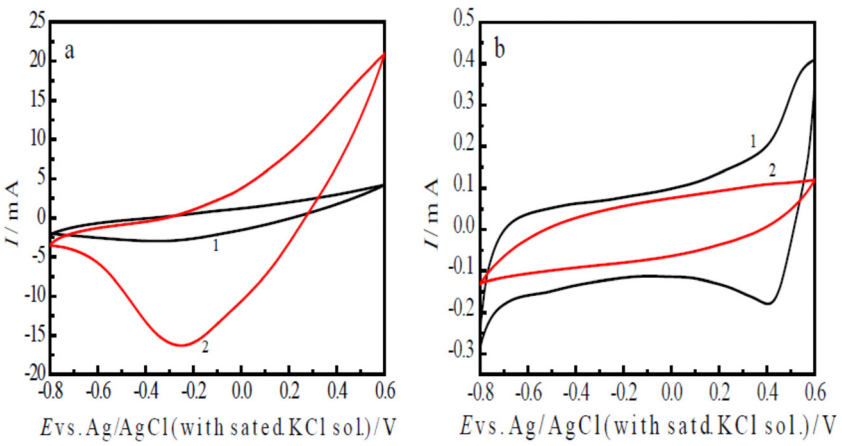

Fig. 4 The CVs of different types of electrodes at a scan rate of 60 mV s^{-1}. (a) Curve 1: nano-PAn/N-graphite electrode in CO_2-saturated water and curve 2: nano-PAn/T-graphite electrode in CO_2-saturated water; (b) curve 1: nano-PAn/T-graphite electrode in a H_2SO_4 solution of pH 3.8 and curve 2: nano-T-graphite electrode in CO_2-saturated water.

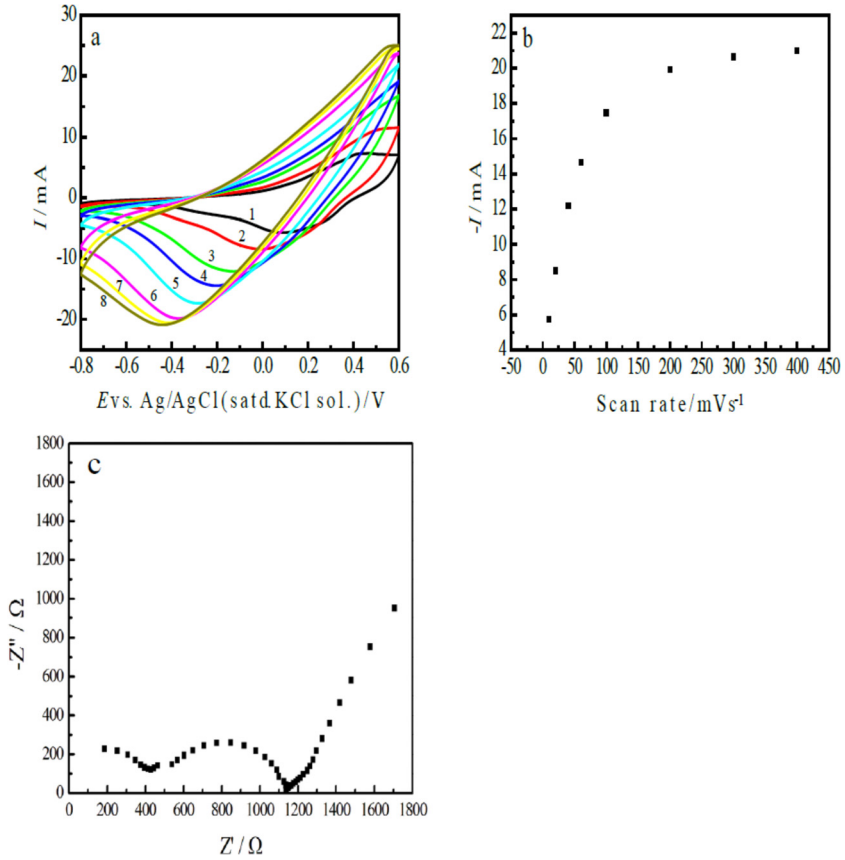

Fig. 5 (a) The CVs of the nano-PAn/T-graphite electrode in CO_2-saturated water free of supporting electrolytes at the following scan rates: (1) 10, (2) 20, (3) 40, (4) 60, (5) 100, (6) 200, (7) 300, and (8) 400 mV s^{-1}; (b) the reduction peak current of CO_2 as a function of the scan rate, based on the data from Fig. 5(a), and (C) the impedance of the nano-PAn/T-graphite electrode at −0.4 V (*vs.* Ag/AgCl with a saturated KCl solution) in CO_2-saturated water free of supporting electrolytes.

On the basis of the results in Fig. 5(a), the relationship between the reduction peak current and the potential scan rate is shown in Fig. 5(b). The results show a linear relationship at scan rates less than 100 mV s^{-1}; this means that the interface charge-transfer process is rate controlling, that is, the electrode reaction rate is controlled by the surface concentration of CO_2 adsorbed on the polyaniline surface at low scan rates. At the high scan rates, the concentration of CO_2 on the electrode surface is not enough to support the rapid electrode reaction, thus deviating from the linear correlation.

As mentioned above, the aniline copolymer/FTO electrode in CO_2-saturated water free of supporting electrolytes shows low reduction current density, which is mainly due to the high resistance (13.3 KΩ) of the solution and FTO, and the high charge transfer resistance (R_{ct} is 124.4 KΩ).[40] Fig. 5(c) presents the impedance plot of the nano-PAn/T-graphite electrode in CO_2-saturated water free of supporting electrolytes; the applied potential was set at −0.40 V. The results indicate that the resistance of the solution and the electrode was 180 Ω, which is much lower than that of the aniline copolymer/FTO electrode, and the charge transfer resistance (R_{ct}) of the nano-PAn/T-graphite electrode was 720 Ω, which is only 1/173 times that of the aniline copolymer/FTO electrode. The difference between the aniline copolymer/FTO electrode and the nano-PAn/T-graphite electrode is mainly due to the different conducting polymers and carriers, that is, since the conductivity of graphite is much higher than that of the FTO semiconductor, and the conductivity of polyaniline is higher than that of the aniline copolymer. In addition, the impedance plot in Fig. 5(c) constitutes a semi-circle and a straight line; this indicates that the regions of mass transfer and kinetic control were at low and high frequencies, respectively; the appearance of a straight line at low frequencies means that the CO_2 reaction on the nano-PAn/T-graphite electrode possessed a fast charge transfer rate, this is due to the fast wettability rate and high wettability of the nano-PAn/T-graphite in the aqueous solution. The reduction current density of CO_2 mainly depends on the resistance and impedance of the electrode system.[6] The above experimental results indicate that the nano-PAn/T-graphite electrode in CO_2-saturated water free of supporting electrolytes shows low resistance and low charge transfer impedance (R_{ct}), which, however, is higher than that of the rGO-CoPc electrode ($R_{ct} \sim 100$ Ω).[45] Therefore, the nano-PAn/T-graphite electrode has rather a high reduction current density for CO_2 electroreduction.

Fig. 5(a) indicates that the reduction peak potential shifted with the scan rate; a reduction peak potential was at −0.44 V at

the scan rate of 400 mV s^{-1}. Clearly, polyaniline shows a low overpotential in the $ERCO_2$. To obtain the product of the electrochemical reduction of CO_2 in CO_2-saturated water free of supporting electrolytes at pH 3.8, the chronoamperometry method was used for the electrochemical reduction of CO_2, and its potential was controlled at −0.45 V based on the result observed in Fig. 5(a). The quantity of electricity consumed during electrolysis over 1000 s was 1.087 C. Considering that polyaniline itself would be reduced during the reduction process at 0.45 V, the reduction of the same polyaniline electrode was carried out at −0.45 V in a very diluted H_2SO_4 solution of pH 3.8, which is equal to that of CO_2-saturated water free of supporting electrolytes; the quantity of electricity consumed for polyaniline reduction was about 0.1 C during electrolysis for 1000 s.

The spectra of ESR and ^{1}H NMR

The $ERCO_2$ is generally considered a free-radical reaction. The initial reaction in CO_2 reduction is the formation of the radical anion.[46]

$$CO_2 + e^- \rightleftharpoons CO_2^{\bullet -}$$

However, the direct detection of the $CO_2^{\bullet -}$ radical in the $ERCO_2$ is scarcely possible because of its short lifetime and especially, since the reduction of CO_2 is carried out in the aqueous solution, water can absorb microwaves, decreasing the ESR signal intensity greatly. Thus, the detection of free radicals in aqueous solutions needs a special ESR cell with a little aqueous solution in the ESR-detecting part of the cell. Because, graphite fibrils broke easily, and the ESR cell was very small, when three electrodes were inserted into the ESR cell, the PAn/T-graphite fibril electrode was broken. Thus, the PAn/Pt electrode was used for ESR measurements. Fig. 6(a) and (b) show the ESR spectra of the same PAn/Pt electrode obtained using the *in situ* electrochemical-ESR technique in the diluted H_2SO_4 solution at pH 3.8 and in the CO_2-saturated water free of the supporting electrolytes at pH 3.8, respectively. Fig. 6(a) and (b) indicate that each ESR spectrum consisted of a single line with a symmetric signal. The *g*-value was 2.0033 in both solutions, which is very close to the value (2.0023) of a free electron. The ESR signals in Fig. 6(a) and (b) are mainly attributed to polyaniline polymerized on the Pt wire. However, the change in ESR signal intensity with applied potential observed in Fig. 6(a) is quite different from that in Fig. 6(b). The ESR signal intensity in Fig. 6(a) decreases with decreasing potential from −0.20 V to −1.2 V. However, the ESR signal intensity in Fig. 6(b) increases with decreasing potential from −0.20 V to −1.2 V. In general, the ESR signal intensity of polyaniline decreases from 0.0 V in

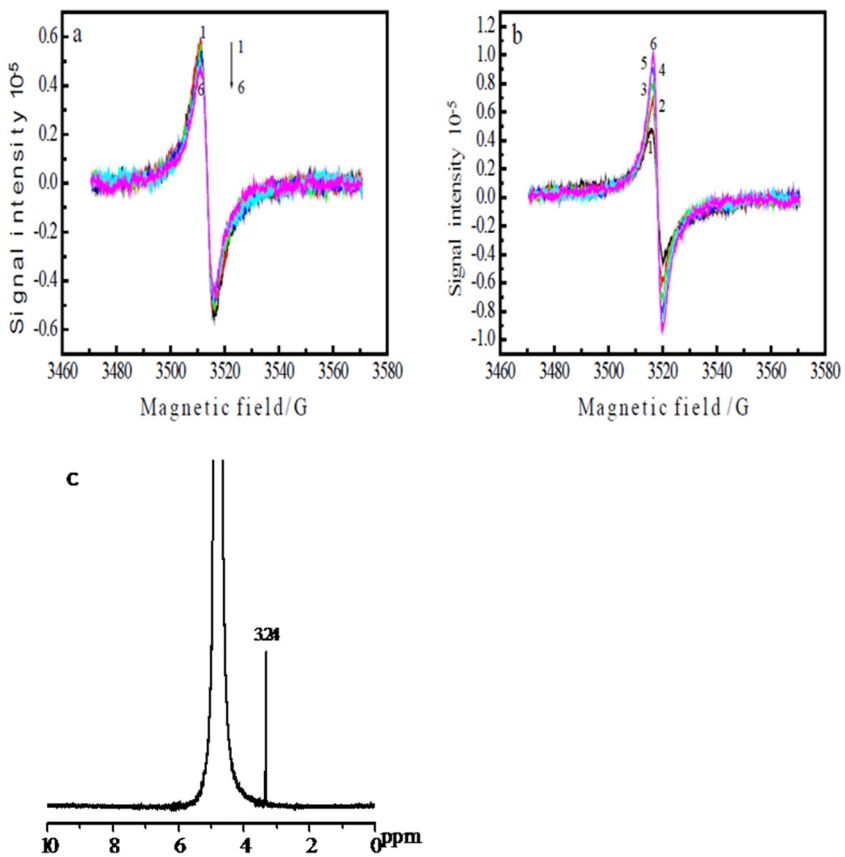

Fig. 6 The ESR spectra of the PAn/Pt electrodes at various potentials (a) in a H_2SO_4 solution of pH 3.8; (b) in CO_2-saturated water free of the supporting electrolyte of pH 3.8 at different potentials: (1) −0.2, (2) −0.4, (3) −0.6, (4) −0.8, (5) −1.0, and (6) −1.2 V (*vs.* Ag/AgCl with a saturated KCl solution); (c) the ^{1}H NMR spectrum of the product solution.

the negative potential direction[47] because the reduction of polyaniline leads to a decrease in radical density. Thus, the increase in ESR signal intensity from −0.20 V to −1.20 V in Fig. 6(b) indicates that a new radical was formed on the polyaniline electrode during the reduction process of CO_2, which should be the $CO^{\bullet-}$ radical anions. However, its ESR spectrum is not separately detected in Fig. 6(b) because CO_2 is adsorbed on polyaniline. Fig. 6(b) is obtained at a constant potential reduction of CO_2 in the potential region of −0.20 V to −1.20 V; the reduction current increases with increasing reduction potential, resulting in an increase in the concentration of the product and free radical in the ESR cell with increasing reduction potential, which leads to the enhancement of the ESR signal intensity when the applied potential changes from −0.20 V to −1.2 V.

Fig. 6(c) presents the ^1H NMR spectrum of the product solution obtained from the reduction of CO_2 at the constant potential of −0.45 V, revealing only one signal in the wide chemical shift region 0–10 ppm except for a D_2O signal. The chemical shift of the methyl protons in methanol is known to be 3.39 ppm;[48] therefore, the signal at 3.24 ppm in Fig. 6(c) is attributed to methanol. Considering the quantity of electricity consumed for the reduction of polyaniline itself, the faradaic efficiency of methanol was approximately 90% (0.987 C/1.087 C), which is higher than that of the aniline copolymer/FTO electrode (66.4%).[40] This demonstrates that the polyaniline catalyst has high faradaic efficiency and high selectivity toward the $ERCO_2$.

The mechanism of CO_2 electroreduction to methanol is rather complicated, because of the six-electron reaction.[17] Here, based on the experiment results, we believe that CO_2 is adsorbed on the surface of the PAn/graphite electrode and the free radical signal is detected in the reduction process of CO_2. A simple mechanism for CO_2 electroreduction in CO_2-saturated water free of supporting electrolytes is suggested as follows:

$$PAn + CO_2(g) \rightarrow PAn/CO_2(ads)$$

$$PAn/CO_2(ads) + 1e^- \rightarrow PAn/CO_2^{\bullet-}(ads)$$

$$PAn/CO_2^{\bullet-}(ads) + 6H^+ + 1e^- \rightarrow CH_3OH + H_2O + PAn$$

Conclusion

In summary, polyaniline deposited on a porous graphite sheet shows good catalytic performance, high selectivity, and a low overpotential. The reduction current density of CO_2 mainly depends on catalyst activity and the resistance and impedance of the electrode system; the nano-PAn/T-graphite electrode in CO_2-saturated water free of supporting electrolytes shows low resistance and low charge transfer impedance (R_{ct}). Therefore, it demonstrates a rather high reduction current density for CO_2 electroreduction. In this work, the $ERCO_2$ was carried out in CO_2-saturated water free of supporting electrolytes, which is environment-friendly and especially, mimics that in which photosynthesis occurs in plants. The free-radical signal was detected during the electrochemical reduction of CO_2 using the *in situ* electrochemical-ESR technique. The $ERCO_2$ was found to be a free radical reaction.

Author contributions

S. L. Mu, the eletrochemical reduction of CO_2, catalyst preparation and, writing paper; Q. F. Shi, the eletrochemical reduction of CO_2 and impedance measurement; C. Chen, ESR measurement; X. X. Gong, physical characterization; H. G. Xue: physical characerization and paper correction.

Conflicts of interest

There are no conflicts to declare.

Acknowledgements

This work was financially supported by the National Nature Science Foundation of China. (grant number 21673203).

References

1 S. Back, H. Kim and Y. S. Jung, Selective heterogeneous CO_2 electroreduction to methanol, *ACS Catal.*, 2015, **5**, 965–971.
2 S. Q. Zhao, S. J. Guo, C. Zhu, J. Gao, H. Li, H. Huang, Y. Liu and Z. H. Kang, Achieving electroreduction of CO_2 to CH_3OH with high selectivity using a pyrite-nickel sulfide nanocomposite, *RSC Adv.*, 2017, **7**, 1376–1381.
3 J. H. Q. Lee, S. J. L. Lauw and R. D. Webster, The electrochemical reduction of carbon dioxide (CO_2) to methanol in the presence of pyridoxine (vitamin B_6), *Electrochem. Commun.*, 2016, **64**, 69–73.
4 X. X. Chang, T. Wang, Z. J. Zhao, P. P. Yang, J. Greeley, R. T. Mu, G. Zhang, Z. M. Gong, Z. B. Luo, J. Chen, Y. Cui, G. A. Ozin and J. L. Gong, Turning Cu/Cu_2O interfaces for the reduction of carbon dioxide to methanol in aqueous solutions, *Angew. Chem., Int. Ed.*, 2018, **130**, 15641–15645.
5 Y. Q. Wang, Z. X. Zhong, T. K. Liu, G. L. Liu and X. L. Hong, Cu@UiO-66 derived Cu^+-ZrO_2 interfacial sites for efficient CO_2 hydrogenation to methanol, *Acta Phys.-Chim. Sin.*, 2021, **37**, 2007089.
6 X. Zhang, J. Fu, Y. Y. Liu, X. D. Zhou and J. L. Qiao, Bismuth anchored on MWCNTs with controlled ultrafine nanosized enables high-efficient electrochemical reduction of carbon dioxide to formate fuel, *ACS Sustainable Chem. Eng.*, 2020, **8**, 4871–4876.
7 P. L. Deng, H. M. Wang, R. J. Qi, J. X. Zhu, S. H. Chen, F. Yang, L. Zhou, K. Qi, H. F. Liu and B. Y. Xia, Bismuth oxides with enhanced bismuth-oxygen structure for efficient electrochemical reduction of carbon dioxide to formate, *ACS Catal.*, 2020, **10**, 743–750.

8 S. W. Wang, T. Y. Kou, J. B. Varley, S. A. Akhade, S. E. Weitzner, S. E. Baker, E. B. Duoss and Y. Li, Cu_2O/CuS nanocomposites show excellent selectivity and stability for formate generation via electrochemical reduction of carbon dioxide, *ACS Mater. Lett.*, 2021, **3**, 100–109.

9 J. T. Feaster, C. Shi, E. R. Cave, T. Hatsukade, D. N. Abram, K. P. Kuhl, C. Hahn, J. K. Noørskov and T. F. Jaramillo, Understanding selectivity for the electrochemical reduction of carbon dioxide to formic acid and carbon monoxide on metal electrodes, *ACS Catal.*, 2017, **7**, 4822–4827.

10 H. D. Manamperi, S. E. Witt and C. Turro, Selective elecrtrocatalytic conversion of CO_2 to HCOOH by a cationic Rh_2(II, II) complex, *ACS Appl. Energy Mater.*, 2019, **2**, 7306–7314.

11 K. Natsui, H. Iwakawa, N. Ikemiya, K. Nakata and Y. Einaga, Stable and highly efficient electrochemical production of formic acid from carbon dioxide using diamond electrodes, *Angew. Chem., Int. Ed.*, 2018, **57**, 2639–2643.

12 X. C. Kang, L. L. Li, A. Sheveleva, X. Han, J. N. Li, L. F. Liu, F. Tuna, E. Mclnnes, B. X. Han, S. H. Yang and M. Schröder, Electro-reduction of carbon dioxide at low over-potential at a metal-organic framework decorated cathode, *Nat. Commun.*, 2020, **11**, 5464.

13 D. Ren, B. Ang and B. S. Yeo, Turning the selectivity of carbon dioxide electroreduction toward ethanol on oxide-derived Cu_xZn catalysts, *ACS Catal.*, 2016, **6**, 8239–8247.

14 K. Zhao, Y. M. Liu, X. Quan, S. Chen and H. T. Yu, CO_2 electroreduction at low overpotential on oxide-derived Cu/carbons fabricated from metal organic framework, *ACS Appl. Mater. Interfaces*, 2017, **9**, 5302–5311.

15 X. Wei, Z. L. Yin, K. J. Lyu, Z. Li, J. Gong, G. W. Wang, L. Xiao, J. T. Lu and L. Zhuang, Highly selective reduction of CO_2 to C_{2+} hydrocarbons at Cu/polyaniline interface, *ACS Catal.*, 2020, **10**, 4103–4111.

16 F. Lü, H. H. Bao, F. He, G. C. Qi, J. Q. Sun, S. S. Zhang, L. C. Zhuo, H. Yang, G. Z. Hu, J. Luo and X. J. Liu, Nitrogen dopant induced highly selective CO_2 reduction over lotus-leaf shaped ZnO nanorods, *Mater. Chem. Front.*, 2021, **5**, 4225–4230.

17 J. L. Qiao, Y. Y. Liu, F. Hong and J. J. Zhang, A review of catalysts for the electroreduction of carbon dioxide to produce low-carbon fuels, *Chem. Soc. Rev.*, 2014, **43**, 631–675.

18 Y. Yan, L. W. Ke, Y. Ding, Y. Zhang, K. Rui, H. J. Lin and J. X. Zhu, Recent advances in Cu-based catalysts for electroreduction of carbon dioxide, *Mater. Chem. Front.*, 2021, **5**, 2668–2683.

19 H. X. Zhong, Y. L. Qiu, T. T. Zhong, X. F. Li, H. M. Zhang and X. B. Chen., Bismuth nanodendrites as a high performance electrocatalyst for selective conversion of CO_2 to formate, *J. Mater. Chem. A*, 2016, **4**, 13746–13753.

20 Y. C. Meng, S. Y. Kuang, H. Liu, Q. Fan, X. B. Ma and S. Zhang, Recent advances in electrochemical CO_2 reduction using copper-based catalysts, *Acta Phys.-Chim. Sin.*, 2021, **37**(5), 2006034.

21 M. Dunwell, Q. Lu, J. M. Heyes, J. Rosen, J. G. Chen, Y. S. Yan, F. Jiao and B. J. Xu, The central role of bicarbonate in the electrochemical reduction of carbon dioxide on gold, *J. Am. Chem. Soc.*, 2017, **139**, 3774–3783.

22 F. Cai, D. F. Gao, R. Si, Y. F. Ye, T. He, S. Miao, G. X. Wang and X. H. Bao, Effect of metal deposition sequence in carbon-supported Pd–Pt catalysts on activity toward CO_2 electroreduction to formate, *Electrochem. Commun.*, 2017, **76**, 1–5.

23 H. Q. Pan and J. Barile, Electrochemical CO_2 reduction on polycrystalline copper by modulating proton transfer with fluoropolymer composites, *ACS Appl. Energy Mater.*, 2022, **5**, 4712–4721.

24 Z. Wang, Y. S. Wu, M. Y. Wang, J. B. Jiang, K. Yang, S. J. Huo, X. F. Wang, Q. Ma, G. W. Brudvig, V. S. Batista, Y. Y. Liang, Z. X. Feng and H. L. Wang, Active sites of copper-complex catalytic materials for electrochemical carbon dioxide reduction, *Nat. Commun.*, 2018, **9**, 415.

25 J. L. Qiao, M. Y. Fan, Y. S. Fu, Z. Y. Bai, C. Y. Ma, Y. Y. Liu and X. D. Zhou, Highly-active copper oxide/copper electrocatalysts induced from hierarchical copper oxide nanospheres for carbon dioxide reduction reaction, *Electrochim. Acta*, 2015, **153**, 559–565.

26 X. L. Jiang, F. Cai, D. F. Gao, J. H. Dong, S. Miao, G. X. Wang and X. H. Bao, Electrocatalytic reduction of carbon dioxide over reduced nanoporous zinc oxide, *Electrochem. Commun.*, 2016, **68**, 67–70.

27 P. Gao, S. G. Li, X. N. Bu, S. S. Dang, Z. Y. Liu, H. Wang, L. S. Zhong, M. H. Qiu, C. G. Yang, J. Cai, W. Wei and Y. H. Sun, Direct conversion of CO_2 into liquid fuels with high selectivity over a bifunctional catalyst, *Nat. Chem.*, 2017, **9**, 1019–1024.

28 K. Saravanan, Y. Basdogan, J. Dean and J. A. Keith, Computational investigation of CO_2 electroreduction on tin oxide and predictions of Ti, V, Nb and Zr dopants for improved catalysis, *J. Mater. Chem. A*, 2017, **5**, 11756–11763.

29 S. L. Mu, J. Wu, Q. F. Shi and F. M. Zhang, Electrochemical reduction of carbon dioxide on nanosized fluorine doped tin oxide in the solution of extremely low supporting electrolyte concentration: Low reduction potentials, *ACS Appl. Energy Mater.*, 2018, **1**, 1680–1687.

30 A. N. Grace, S. Y. Choi, M. Vinoba, M. Bhagiyalakshmi, D. H. Chu, Y. Yoon, S. C. Nam and S. K. Jeong, Electrochemical reduction of carbon dioxide at low overpotential on a polyaniline/Cu_2O nano composite based electrode, *Appl. Energy*, 2014, **120**, 85–94.

31 A. Loiudice, P. Lobaccaro, E. A. Kamali, T. Thao, B. H. Huang, J. W. Ager and J. Buonsanti, Tailoring copper nanocrystals towards C_2 products in electrochemical CO_2 reduction, *Angew. Chem., Int. Ed.*, 2016, **55**, 5789.

32 S. Gao, Y. Lin, X. C. Jiao, Y. F. Sun, Q. Q. Luo, W. H. Zhang, D. Q. Li, J. L. Yang and Y. Xie, Partially oxidized atomic cobalt layers for carbon dioxide electroreduction to liquid fuel, *Nature*, 2016, **529**, 68–72.

33 F. C. Lei, W. Liu, Y. F. Sun, J. Q. Xu, K. T. Liu, L. Liang, T. Yao, B. C. Pan, S. Q. Wei and Y. Xie, Metallic tin quantum sheets confined in graphene toward high-efficiency carbon dioxide electroreduction, *Nat. Commun.*, 2016, **7**, 12697.

34 Y. Zhao, X. Tan, W. F. Yang, C. Jia, X. J. Chen, W. H. Ren, S. C. Smith and C. A. Zhao, Surface reconstruction of ultrathin palladium nanosheets during electrocatalytic CO_2 reduction, *Angew. Chem., Int. Ed.*, 2020, **59**, 21493–21498.

35 C. H. Wang, C. M. Li, J. L. Liu and C. X. Guo, Engineering transition metal-based nanomaterials for high-performance electrocatalysis, *Mater. Rep.: Energy*, 2021, **1**, 100006.

36 J. W. Wang, Y. P. Zheng, W. Ren, E. H. Arg, L. Song and J. X. Zhu, Intrinsic ionic confinement dynamic engineering of ionomers with low dielectric-K, high healing and stretchability for electronic device reconfiguration, *Chem. Eng. J.*, 2022, 139837.

37 H. D. Liu, C. F. Du, L. L. Liao, H. J. Zhang, H. Q. Zhou, W. C. Zhou, T. N. Ren, Z. H. Sun, Y. F. Lu, Z. T. Nie, F. Xu, J. X. Zhu and W. Huang, Approaching intrinsic dynamics of MXenes hybrid hydrogel 3D printed multimodal intelligent devices with ultrahigh superelasticity and temperature sensitivity, *Nat. Commun.*, 2022, **13**, 3420.

38 F. L. Yang, D. L. Hegh, D. X. Song, J. Z. Zhzng, K. A. S. Usman, C. Liu, Z. Y. Wang, W. G. Machine, W. R. Yangon, S. Qin and J. M. Razal, Synthesis of nitrogen–sulfur co-doped Ti_3C_2Tx MXene with enhanced electrochemical properties, *Mater. Rep.: Energy*, 2022, **2**, 100079.

39 S. Ringe, C. G. Morales-Guio, L. D. Chen, M. Fields, T. F. Jaramillo, C. Hahn and K. Chan, Double layer charging driven carbon dioxide adsorption limits the rate of electrochemical carbon dioxide reduction on gold, *Nat. Commun.*, 2020, **11**, 33.

40 J. Wu, Q. F. Shi and S. L. Mu, Synthesis of aniline copolymer and as an active catalyst layer for electrochemical reduction of carbon dioxide in water free of supporting electrolytes, *Synth. Met.*, 2019, 255.

41 M. Li, M. N. Idros, Y. M. Wu, T. Burdyny, S. Garg, X. S. Zhao, G. Wang and T. E. Rufford, The role of electrode wettability in electrochemical reduction of carbon dioxide, *J. Mater. Chem. A*, 2021, **9**, 19369–19409.

42 F. M. Zhang and S. L. Mu, Influence of potential and temperature on the ESR spectra of polyaniline synthesized using the interface polymerization, *J. Phys. Chem. B*, 2010, **114**, 16687–16693.

43 W. S. Huang, B. D. Humphrey and A. G. MacDiarmid, Polyaniline, a novel conducting polymer, *J. Chem. Soc., Faraday Trans. 1*, 1986, **82**, 2385–2400.

44 A. AlRatrout, M. J. Blunt and B. Bijeljic, Wettability in complex porous materials, the mixed-wet state, and its relationship to surface roughness, *Proc. Natl. Acad. Sci. U. S. A.*, 2018, **115**, 8901–8906.

45 F. X. Liang, J. Zhang, Z. W. Hu, C. Ma, W. P. Ni, Y. Zhang and S. Zhang, Intrinsic defect-rich graphene coupled cobalt phthalocyanine for robust electrochemical reduction of carbon dioxide, *ACS Appl. Mater. Interfaces*, 2021, **13**, 25523–25532.

46 T. H. Kai, M. Zhou, Z. Y. Duan, G. A. Henkelman and A. J. Bard, Detection of $CO_2^{\bullet-}$ in the electrochemical reduction of carbon dioxide in *N*,*N*-dimethylformamite by scanning electrochemical microscopy, *J. Am. Chem. Soc.*, 2017, **139**, 18552–18557.

47 Y. F. Li and S. L. Mu, *The Electrochemistry of the Conducting Polymers (Chinese)*, Sciences Press, Beijing, 2020, pp. 63–67.

48 E. Pretch, P. Bühlmann and C. Affolter, *Strruture of Determination of Organic Compounds*, Springer-Verlag, Berlin, 2000.

